JMB

Yeast D-Amino Acid Oxidase: Structural Basis of its Catalytic Properties

Loredano Pollegioni¹, Kay Diederichs², Gianluca Molla¹ Stephan Umhau², Wolfram Welte², Sandro Ghisla² and Mirella S. Pilone¹*

¹*Department of Structural and Functional Biology University of Insubria via J.H. Dunant, 3 21100 Varese, Italy*

²*Section of Biology University of Konstanz P.O. Box 5560-M644 D-78457 Konstanz, Germany*

*Corresponding author

The 3D structure of the flavoprotein D-amino acid oxidase (DAAO) from the yeast *Rhodotorula gracilis* (RgDAAO) in complex with the competitive inhibitor anthranilate was solved (resolution 1.9 Å) and structural features relevant for the overall conformation and for catalytic activity are described. The FAD is bound in an elongated conformation in the core of the enzyme. Two anthranilate molecules are found within the active site cavity; one is located in a funnel forming the entrance, and the second is in contact with the flavin. The anchoring of the ligand carboxylate with Arg285 and Tyr223 is found for all complexes studied. However, while the active site group Tyr238-OH interacts with the carboxylate in the case of the substrate D-alanine, of D-CF₃-alanine, or of L-lactate, in the anthranilate complex the phenol group rotates around the C2–C3 bond thus opening the entrance of the active site, and interacts there with the second bound anthranilate. This movement serves in channeling substrate to the bottom of the active site, the locus of chemical catalysis. The absence in RgDAAO of the "lid" covering the active site, as found in mammalian DAAO, is interpreted as being at the origin of the differences in kinetic mechanism between the two enzymes. This lid has been proposed to regulate product dissociation in the latter, while the side-chain of Tyr238 might exert a similar role in RgDAAO. The more open active site architecture of RgDAAO is the origin of its much broader substrate specificity. The RgDAAO enzyme forms a homodimer with *C*2 symmetry that is different from that reported for mammalian D-amino acid oxidase. This different mode of aggregation probably causes the differences in stability and tightness of FAD cofactor binding between the DAAOs from different sources.

© 2002 Elsevier Science Ltd. All rights reserved

Keywords: D-amino acid oxidase; crystal structure; anthranilate; dimerization mode; substrate access
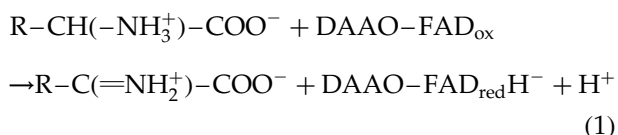
Introduction

D-Amino acid oxidase (DAAO, EC 1.4.3.3) was one of the first flavoproteins to be discovered in the mid-30s of the last century[1] and has played a
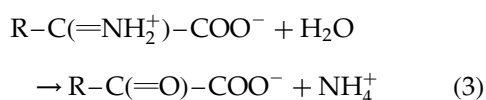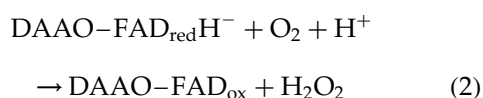
prominent role in the development of present concepts in mechanistic flavin enzymology. It is a peroxisomal enzyme that catalyses the deamination of D-amino acid residues to their imino acid counterparts with concomitant reduction of FAD (see equation (1)). The reduced flavin is subsequently re-oxidized by molecular oxygen generating H₂O₂ (equation (2)), and the imino acid is released into solvent where it spontaneously hydrolyses to the corresponding α-keto acid and ammonia (equation (3)):

$$R-CH(-NH_3^+)-COO^- + DAAO-FAD_{ox}$$

$$\rightarrow R-C(=NH_2^+)-COO^- + DAAO-FAD_{red}H^- + H^+$$

$$(1)$$

$$DAAO-FAD_{red}H^- + O_2 + H^+$$

$$\rightarrow DAAO-FAD_{ox} + H_2O_2 \quad (2)$$

$$R-C(=NH_2^+)-COO^- + H_2O$$

$$\rightarrow R-C(=O)-COO^- + NH_4^+ \quad (3)$$

In yeast cells, the flavoprotein DAAO is involved in primary metabolism where the efficiency of D-amino acid utilization is fundamental for cell growth.[2,3] Conversely, in higher organisms, where its reaction occurs in selected organs, the physiological function is not entirely clear. In kidney it is probably involved in detoxification of exogenous D-amino acid residues,[4] and good arguments for a role in neurotransmission regulation in brain have been advanced recently.[5] DAAO also has considerable biotechnological importance for the enzymatic conversion of cephalosphorin C into 7-amino cephalosporanic acid.[6]

Yeast and mammalian DAAOs share features such as the basic catalytic mechanism. However, they differ in important aspects such as catalytic efficiency, substrate specificity, aggregation state, stability, kinetic mechanism, and mode and effectiveness of FAD binding. Thus, DAAO from the yeast *Rhodotorula gracilis* (RgDAAO) has a k_{cat} value $\approx 20,000$ minute^{-1} compared to 600 minute^{-1} for pig kidney DAAO (pkDAAO) with D-alanine as substrate.[7,8] This diversity arises mainly from a different rate-limiting step in the catalytic cycle. It is flavin reduction with RgDAAO,[7] and product release with pkDAAO.[8] Yeast DAAO can utilize large substrates such as cephalosporin C, this being only marginally the case with mammalian DAAO.[9] While yeast DAAO exists in a stable dimeric state, pkDAAO dissociates easily and releases the FAD cofactor concomitant with loss of activity. The understanding of the molecular basis for these similarities and differences was the rationale for the present work.

In 1996, the 3D structure of pkDAAO at a 2.5–3.0 Å resolution was reported.[10,11] We have subsequently obtained the structure of the yeast enzyme, RgDAAO at 1.2–1.7 Å resolution and have reported on some aspects of mechanistic significance.[12] This, together with site-directed mutagenesis and mechanistic studies from our groups,[13–16] has resulted in the conclusion that dehydrogenation by DAAO occurs *via* a hydride transfer.[12] The 3D structure of L-amino acid oxidase (LAAO) also has been reported recently,[17] and this provides the basis for an understanding of the molecular factors leading to substrate D, or L-specificity.

Here we address the questions mentioned above pertaining to the similarities and differences between the yeast and mammalian DAAOs. In this context we present the crystal structure of RgDAAO in complex with the competitive inhibitor anthranilate (*o*-aminobenzoate). This molecule has attained mechanistic significance, since it was found to form the so-called "purple complexes"

upon binding to pkDAAO,[9] and has been used widely as a model inhibitor. The structures of pkDAAO and LAAO in complex with anthranilate have also been solved;[17,18] it was thus expected that comparisons of the modes of interaction of this ligand with the three enzymes would provide insights into similarities and differences of structure–function relationships of these flavoenzymes. We also address the factors that determine catalytic efficiency and the stability of the dimeric forms of DAAO.

Results

Overall structure and topology

The RgDAAO used here is a chimeric protein containing six additional residues (MARIRL) at the N terminus[19] in addition to the 368 amino acid residues of the native form.[20] The 3D structure of the complex obtained in the presence of anthranilate is depicted in Figure 1. Secondary structure elements have been adapted and named according to the topology described by Mattevi *et al.*[10] and some important elements are indicated. While there is correspondence between the FAD-binding domain (denoted with F) for the RgDAAO and pkDAAO, the interface domains (denoted with I) are different, leading to a different mode of dimer formation (see below). For simplicity and ease of comparison we have nevertheless retained the original nomenclature[10] for the interface domains. The secondary structure topology, consists of 11 α-helices and 13 β-strands; it is overall analogous to that of pkDAAO.[10,11] The polypeptide chain has an irregular disposition and frequently crosses between the two domains whose main structural elements are central antiparallel β-sheets. Compared to pkDAAO, in the "head" region of RgDAAO there are three additional short α-helices: based on the terminology used by Mattevi *et al.*[10] these can be named αI1′ (between βI1 and βI2), αI3′ and αI3″ (both after αI3). Two main topological differences are also evident: the presence of a significantly shorter (six residues in RgDAAO *versus* 11 residues in pkDAAO) active site loop connecting βI5 and βI6 (Figure 1), and the presence of a long C-terminal loop (21 amino acid residues connecting βF5 and βF6), not present in other known DAAO sequences (see highlighted segments in Figures 1, 4 and 5). The functional effects of these structural differences will be discussed in detail below.

By structural overlay, the RgDAAO structure was compared to that of other flavoprotein oxidases (see Table 1). On the basis of structural and sequence homologies,[20,21] RgDAAO can be classified as a member of the large glutathione reductase (GR) family (all the family members adopt the Rossmann fold[22,23]), and therein into the subgroup GR$_2$ which was reported to show sequence similarity mainly within 30 residues in the N-terminal
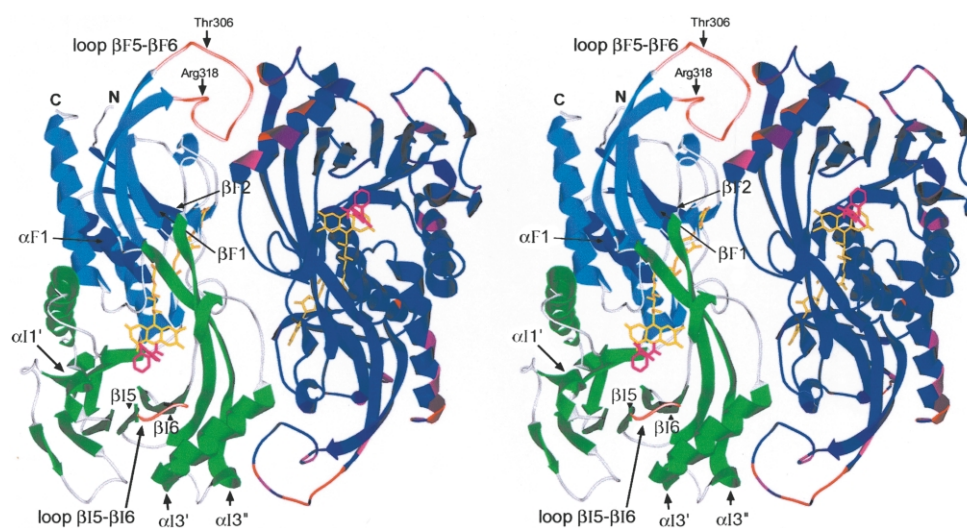
Figure 1. Ribbon representation of RgDAAO−anthranilate complex. The picture depicts the proposed dimer (see also Figure 3). In the monomer on the left-hand-side the "flavin-binding domain" is depicted in blue and the interface domain in green. The same terminology as introduced by Mattevi *et al*. for pkDAAO[10] has been used in order to facilitate comparison between the two proteins. The segments in red denote two additional loops not present in pkDAAO; the βF1−αF1−βF2 secondary elements corresponding to the βαβ motif of the Rossmann fold[22] (the dinucleotide-binding motif[25,26]) are shown in dark blue. Arrows indicate the peptide bonds sensitive to proteolytic attack.[24,34] The carbon atoms of the FAD cofactor are in yellow and those of the two anthranilates inside the active site in magenta. The monomer on the right is represented using a color scaling for temperature factors: blue corresponds to a low *B*-factor and red to a high value.

region.[23] Our superimposition procedure identifies significantly larger structurally homologous parts. However, in the case of the comparisons of RgDAAO and pkDAAO, the r.m.s. deviation of 1.38 Å for 281 superimposable C^α atoms (within a 3.5 Å cut-off) is surprisingly high and reflects the evolutionary distance between the mammalian and the yeast enzyme. On the other hand, it is in accord with the relatively low percentage of identical residues (31.8%) in the superimposed regions.

The closest structural relative of DAAO within the GR$_2$ family is sarcosine oxidase. Indeed the two enzymes have identical topologies. In this case, the superimposed regions encompass sequence sections that are disposed over the whole sequence, whereas the other members of the GR$_2$ family mainly superimpose in their N-terminal region.[23] No correlation between the r.m.s. deviation and the percentage of superimposed residues is evident from comparing

RgDAAO with other GR$_2$ family members. This might hint at the large mutual evolutionary distance of members within this family, their broad range of substrate specificities and concomitant mechanistic peculiarities. High topological similarity is found within the GR$_2$ family in the "flavin-binding domain" (Figure 1). In contrast only parts of the "interface domain" can be superimposed in pair-wise fashion.

N and C termini

At the N terminus only two (RL) out of six of the additional amino acid residues (MARIRL) can be modelled into the electron density, the remaining four apparently possessing a flexible conformation. This segment appears to be a significant component in crystal formation and growth, since we have failed to obtain crystals of wild-type (368 amino acid residues) protein. The backbone of residues Leu1 and Met1 (the original N-terminal

Table 1. Comparison of structural features of RgDAAO with other members of the GR$_2$ family[23]

Protein (PDB accession code)	Number of residues within 3.5 Å cutoff	r.m.s. deviation of residues within 3.5 Å cutoff	Sequence identity of residues within 3.5 Å cutoff (%)
pkDAAO (1aa8)	281	1.38	31.8
Sarcosine oxidase (1b3m_a)	193	1.66	18.7
Phenol hydroxylase (1foh)	121	1.75	17.4
p-Hydroxybenzoate hydroxylase (1bf3)	120	1.65	19.2
L-Amino acid oxidase (1f8r)	120	1.70	24.4
Cholesterol oxidase (1b4v)	110	1.87	20.4
Glucose oxidase (1cf3)	108	1.83	18.7
Polyamine oxidase (1b37_a)	99	1.47	22.4
Fumarate reductase (1d4c_a)	97	1.58	26.8

residue of the wild-type protein) makes H-bonds with two backbone residues Ala296 and Arg298 of the β-strand F5 of a symmetry-related protein molecule. Furthermore, the backbone carbonyl of His2 is H-bonded to Arg358, and Met1 is also in van der Waals contact with Val351 and Tyr359 of α-helix αF5 of the same symmetry-related molecule. Buried surfaces have been calculated using both the complete coordinates and a modelled protein lacking the additional N-terminal sequence. In this latter case, the buried surface area between the monomers in crystal contact is decreased by $\sim 700\ \text{Å}^2$ in comparison to the value determined using the complete coordinates.

Flexible parts

In the long loop connecting βF5 and βF6 (Figure 1) the electron density for eight amino acid residues (Arg312–Gln319) is weak, indicating that part of the loop is very flexible. As was the case with pkDAAO,[10,11] the C-terminal residues Ala362–Leu368 are also not visible in the electron density. This region contains the SKL tripeptide, corresponding to the PTS1 targeting sequence for peroxisomal proteins. This observation highlights the importance of the flexibility in the targeting signal for interaction with the PAS8-like receptor, the peroxisomal membrane protein that selectively binds the SKL peptide of peroxisomal proteins on the cytosolic face of peroxisomes. This part of the RgDAAO sequence is highly susceptible to proteolysis *in vivo*. The enzyme purified from *R. gracilis* cells consists of three isoforms when analysed by isoelectrofocusing.[24] The microheterogeneity stems from the association of two polypeptide chains differing in the C-terminal tripeptide, giving rise to three different holoenzyme dimers.[24]

## FAD binding

The FAD-binding patterns of RgDAAO and pkDAAO share an overall similarity while exhibiting some substantial differences. In both DAAOs the domain contains the conserved consensus Rossmann fold[22] βαβ motif (βF1, αF1, βF2), known as the dinucleotide-binding motif,[25,26] common within FAD and NAD(P)H-dependent oxidoreductases.[23,27] The central part of this consensus motif is the sequence GXGXXG (Gly11, 13 and 16 of helix αF1) with the N-terminal end of helix αF1 pointing toward the FAD pyrophosphate moiety. This serves in charge compensation, as observed for other dinucleotide-binding proteins.[25] The residues interacting with the pyrophosphate oxygen atoms are more conserved compared to other segments,[20] highlighting the importance of this interaction for cofactor recognition.[20,23] The FAD in RgDAAO is found in an extended conformation typical of this GR family.[23] The whole cofactor is buried inside the protein (Figure 1) and is not solvent accessible in agreement with previous deductions based on the absence of reac-

tivity of enzyme reconstituted with modified FAD analogues with solvent-born reagents.[28] The isoalloxazine ring is located at the interface of the two domains, with the *re*-side facing the inner part of the substrate-binding cavity. The large majority of the potential FAD H-bonds are with the protein, thus resulting in a tight net, as shown in Figure 2. The three rings of the isoalloxazine system form an almost perfect plane, wherein only the C(2)=O and C(4)=O groups occupy a slight "out-of-plane" position. As reported,[12] the oxidized and reduced forms of the flavin do not differ significantly in their structural features and position. The flavin ring is held in position by a H-bond pair from its N(3)H–C(4)=O to the Asn54 amide while N(5) is within H-bond distance to Gly52α–NH (both residues are located on the loop region connecting β-strand F2 with α-helix αI1). The flavin N(1) is within H-bond distance with Ser335(=O), such an interaction being absent in pkDAAO. The environment of the O(2) position is substantially different between RgDAAO and pkDAAO: in the latter the partial positive charge of a dipole induced by helix αF5 is assumed to concur in the stabilization of the negative charges of the reduced flavin. Such a feature is absent in RgDAAO: O(2) forms two tight H-bonds with the backbone NH groups of Gln339 and Tyr338, both residues belonging to helix αF5, while in pkDAAO O(2) interacts with a threonine[10] (Figure 2). The hydrophobic part of the isoalloxazine ring makes van der Waals contacts with a pocket formed by the antiparallel β-strands I6 and I7 and interacts specifically with residues Ala51, Trp50, Gly183, Gly199, Thr201, Tyr223, and Arg285. The FAD diphosphate group forms H-bonds with Ala47, Ser48 and additionally with Ile15, the residue located at the beginning of the helix αF1, and the helix dipole is assumed to contribute to the stabilization of the two negative charges of the diphosphate, as found with other members of the GR family.[23] Four water molecules are found at optimal distance for H-bond formation with three of the phosphate oxygen atoms (Figure 2). This is different from pkDAAO, where only three water molecules interact with two of the phosphate oxygen atoms.[10,11] The highly conserved Asp34 of the mononucleotide-binding domain interacts *via* two strong H-bridges with two OH groups of the AMP ribosyl moiety. One of these is also H-bonded with the backbone N of Ser12, while the adenine moiety interacts with the backbone of Val162 and Arg35, and this gives the rationale of the observation that RgDAAO cannot productively use FMN[28] (Figure 2). Thus, although different amino acid residues interact with AMP in yeast and the mammalian enzyme, the overall picture is similar in the two DAAOs.

Mode of dimerization

Native DAAO from *R. gracilis* is a stable 80 kDa dimer of identical subunits, independent of the
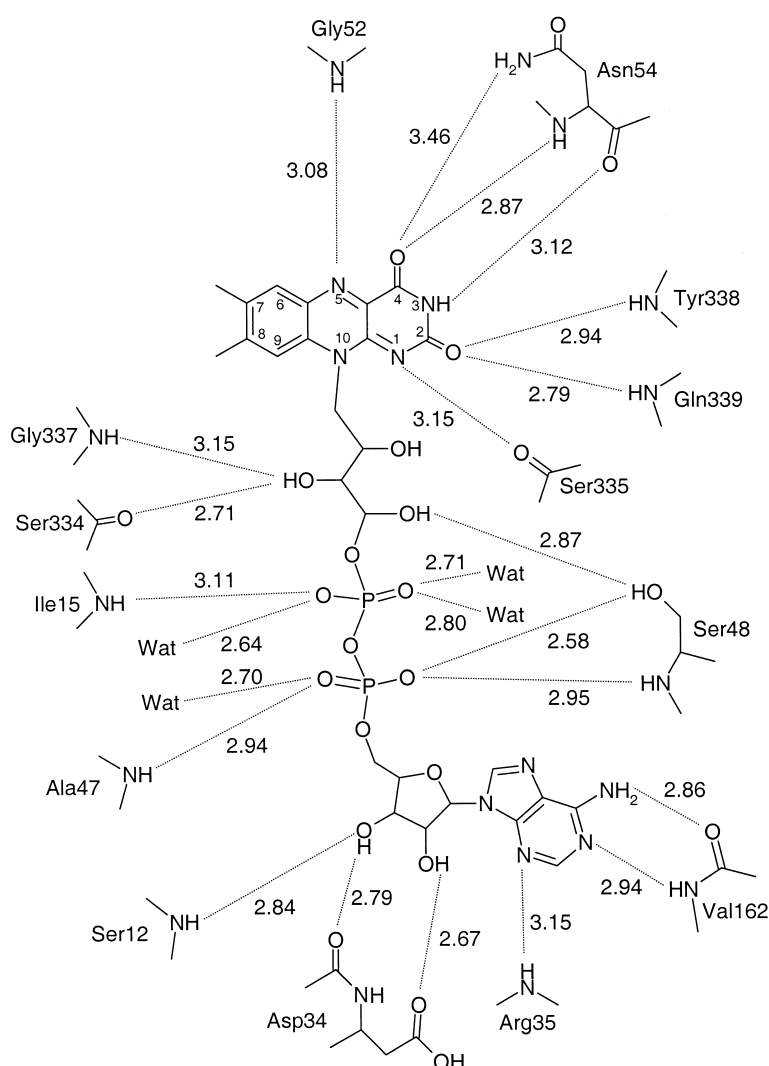
Figure 2. Schematic representation of the flavin–apoprotein interactions in RgDAAO. View on the *si*-face of the flavin. Residues interacting with donor or acceptor atoms of the cofactor are depicted. The hydrogen bonds are marked as dotted lines (distances are in Å).

protein concentration.[29] Each monomer contains one non-covalently bound FAD molecule.[29] In contrast to this, the apoprotein form of RgDAAO is monomeric and rapidly converts to dimeric holoenzyme upon addition of FAD.[30] Considering that the FAD cofactor is involved in many protein core contacts (see above), it is deduced that dimerization follows holoenzyme reconstitution. The dimer molecular mass estimated by dynamic light scattering is ∼79 kDa and thus in accordance with a theoretical value of 82 kDa for the recombinant RgDAAO.[19] This is consistent with RgDAAO forming a roughly spherical homodimer in solution. All crystals of RgDAAO have the tetragonal space group *I*422 and approximate cell axes $a = b = 121$ Å and $c = 136$ Å. The mode of dimerization cannot be derived directly from space group crystal symmetry under these circumstances.

In the 3D structure, the monomer of the asymmetric unit makes crystal contacts to give three symmetry-related dimers, indicating different, possible modes of monomer–monomer interaction (see Figures 1 and 3). For all the resulting potential dimers, the surface buried by the contact area was calculated using the CNS software package.[31] For the "side to side" dimer, the buried surface area at the interface of two monomers was calculated as 678 Å² (Figure 3(a)). In analogy to the case of pkDAAO, also for RgDAAO a "head to head" mode of dimerization has to be discussed (compare Figure 3(b) and (c)). In this case the monomers would be related by a 2-fold axis with approximately 15% (1492 Å²) of the monomer accessible surface buried upon dimerization, yielding an elongated dimer of cylindrical shape (112 Å × 45 Å × 31 Å). This value is nearly the same as that reported for the pkDAAO dimer, where the buried surface area is 1512 Å² (Figure 3(c)).[10] The largest buried surface (3049 Å²) is, however, obtained for a "head to tail" monomer orientation with 2-fold symmetry (Figure 1) leading to

A) side to side   B) head to head   C) pkDAAO head to head
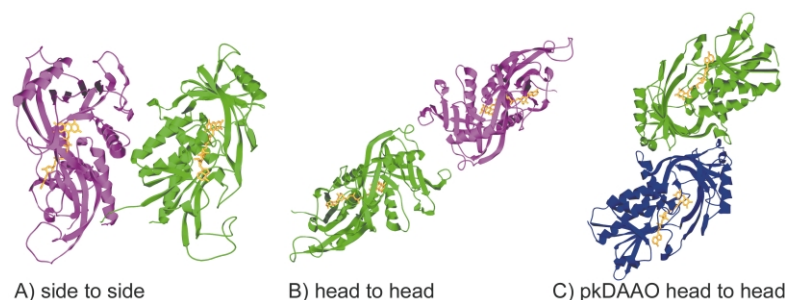
Figure 3. Possible, alternative modes of monomer–monomer interaction of DAAO from crystal contacts. (a) The "side to side" mode of dimer formation. This has the smallest buried surface area (see the text). (b) RgDAAO in the alternate head to head mode of dimerization. (c) The head to head mode of dimerization proposed for pkDAAO[10,11] is shown for comparison. The head to tail mode of dimer formation proposed for RgDAAO is depicted in Figure 1.

the suggestion that this is the dimer form present in solution. Notably, loop βF5–βF6 of yeast DAAO is not conserved in other DAAO sequences.[20] The mean overall *B*-factors of RgDAAO are $\approx 15\ \text{Å}^2$, i.e. low (Figure 1). Only a few loop regions show slightly higher values such as residues 303–313 of the long loop connecting β-strands F5 and F6. However, the residues of this loop that are involved in crystal contact and con-

tribute to dimer formation in the head to tail dimer have *B*-factors comparable to the mean.

The active site cavity

The active site of RgDAAO is a cavity delimited by the two long β-strands I4 and I8 bent around the isoalloxazine ring of the flavin and the two short β-strands I5 and I6 situated close to the
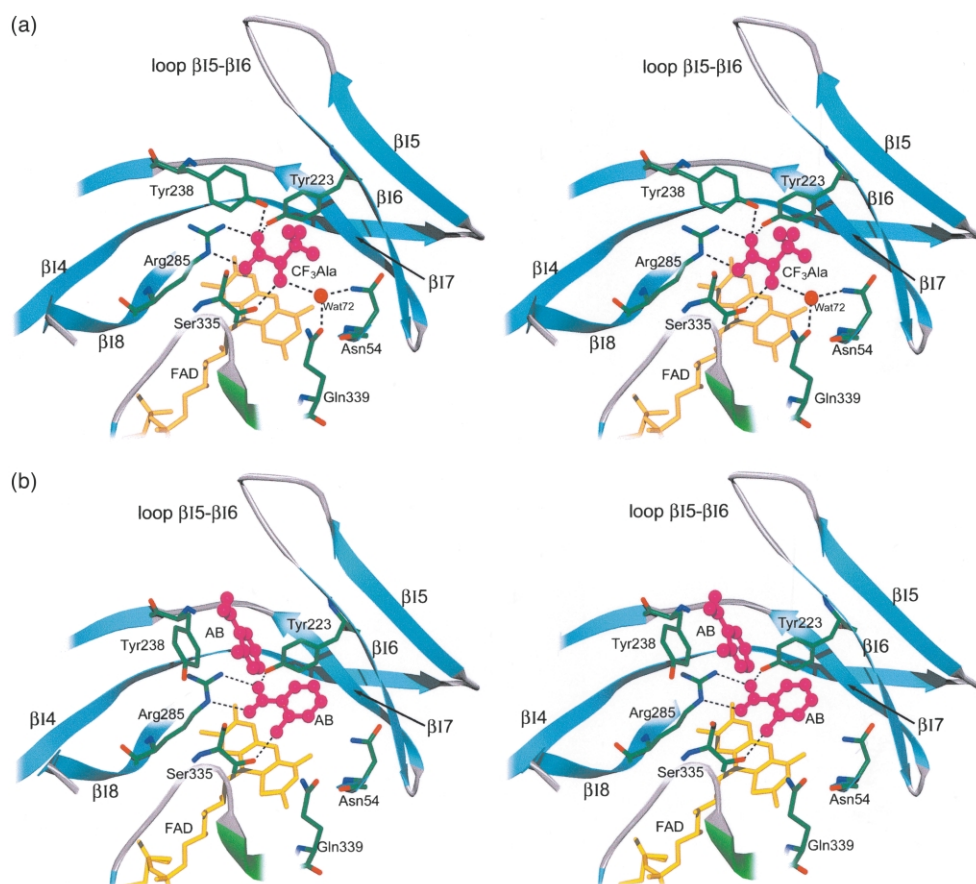
Figure 4. (a) Ligand–active site interactions of RgDAAO. The ligand bound is CF₃-D-Ala (shown in magenta). Broken lines denote hydrogen bonds. Note the absence at the active site of functional groups that could participate in chemical events. (b) The active site region of RgDAAO in complex with anthranilate showing the channeling of two molecules of anthranilate (shown in magenta) into the active site cavity (Wat72 is no more present).
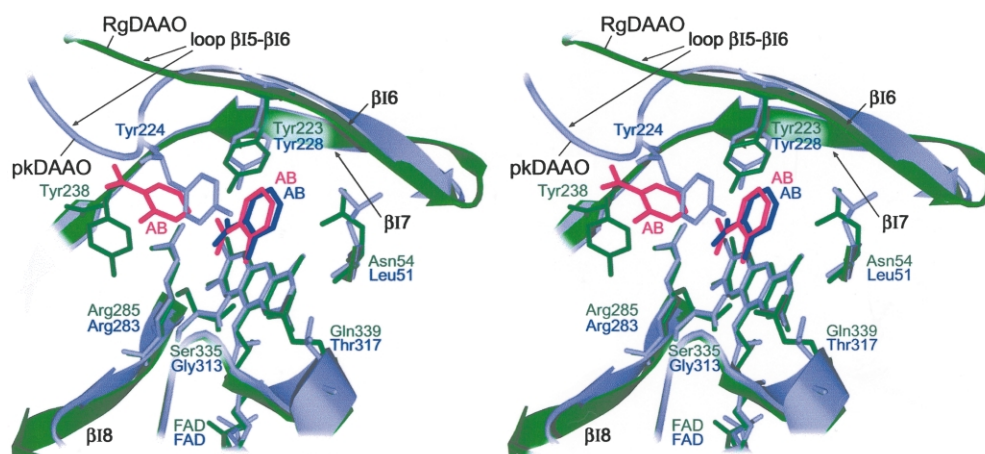
Figure 5. Comparison of the active site of RgDAAO and pkDAAO, both complexed with anthranilate. Features of the RgDAAO structure are in green, those of pkDAAO in light blue. The two molecules of anthranilate bound to RgDAAO are shown in magenta. The single anthranilate molecule bound to pkDAAO is in blue.

substrate-binding site (see Figure 4(a)). The flavin forms the "bottom" of the cavity. All these β-strands have an antiparallel orientation and are connected to each other by H-bonds resulting in a rather rigid arrangement. At the *re*-side of the flavin, the loop connecting β-strand F2 and helix αI1 is involved in backbone H-bonds with flavin functional groups (see above). On the *si*-side, the N-terminal end of the long helix αF5 forms the boundary of the active site (see Figure 4). Interestingly the loop found in pkDAAO, which was proposed by Mattevi *et al*. to act as a "lid" controlling access to the active site[32] is absent in RgDAAO (see below). This loop contains an important residue, Tyr224, that is probably involved in substrate/product fixation[33] and interacts with the substrate α-amino group and an active site water molecule. In RgDAAO the Tyr238 side-chain is placed at a similar position (Figures 4 and 5). Tyr238 is, however, located on a different segment of the chain, the loop connecting βI7 and αI3.

The side-chains of the residues involved in substrate binding and fixation, including Wat72, retain the same positions in three of the complexes studied, CF_3-D-Ala, L-lactate and D-alanine (Figure 4(a)). The interactions can be described as follows: (a) Arg285 forms a pair with the α-COO⁻ of the substrate, and both Tyr223-OH and Tyr238-OH interact with one of its oxygen atoms probably preventing rotation; (b) Ser335α-NH and Wat72 (held in position by Asn54 and Gln339) fix the ligand αNH_2/OH *via* a short and symmetric pair of H-bonds (both 2.72 Å); (c) the fourth, and frequently largest ligand αC substituents, occupies the space provided by the active site cavity and extends towards its entrance. We have compared the substrate-binding modes by superimposing the 3D structures of RgDAAO (complexed with D-alanine or anthranilate), pkDAAO (with anthranilate)[10,11] and LAAO[17] (with anthranilate) while keeping the flavin moiety constant. The superposition of the active centre of pkDAAO and

RgDAAO in complex with anthranilate is shown in Figure 5 and will be discussed below.

The anthranilate complex

Two molecules of anthranilate are found at the active site in crystals soaked with this competitive inhibitor (Figures 1, 4(b) and 5). One is placed in the vicinity of the flavin N(5), at a position similar to that occupied by D-alanine, and the second is located at the entrance of the active centre cavity. Comparison of the binding mode of the first anthranilate with that of D-alanine, CF_3-D-Ala, and L-lactate (Figures 4 and 5) shows that all of these ligands are located at similar positions, the H-bond interactions and conformation of Arg285, Tyr223 and Ser335 being essentially identical. From this it follows that the substrate αC−H is placed in the extension of the N(5) LUMO orbital of the flavin on its *re*-side.[12] However, two significant differences are also evident: in the RgDAAO–anthranilate complex, Tyr238 has moved away from the ligand −COO⁻ and it is too distant to make any discrete H contact(s) with the latter. Furthermore, the active site water W72, which forms an H-bond with the OH/NH_2 function of the other ligands, is not found in the DAAO–anthranilate complex. The aromatic ring of anthranilate is in contact with the hydrophobic residues (Ile225, Phe58, Tyr223) within the binding pocket, possibly contributing to the overall binding enthalpy (anthranilate binding, $K_d \approx 2$ mM, is relatively tight compared e.g. to D-lactate, 16 mM). Displacement of Wat72 in the DAAO–anthranilate complex is due to the bulkiness of the ligand. The second anthranilate molecule lies parallel with, and in contact with, Tyr238, the latter having modified its position compared to that in the structures of the other complexes (Figures 4 and 5). The side-chains of Phe58, Ser215, Pro221, and the backbone of Ser234 and Ser235 form the entrance to the active site whose opening is
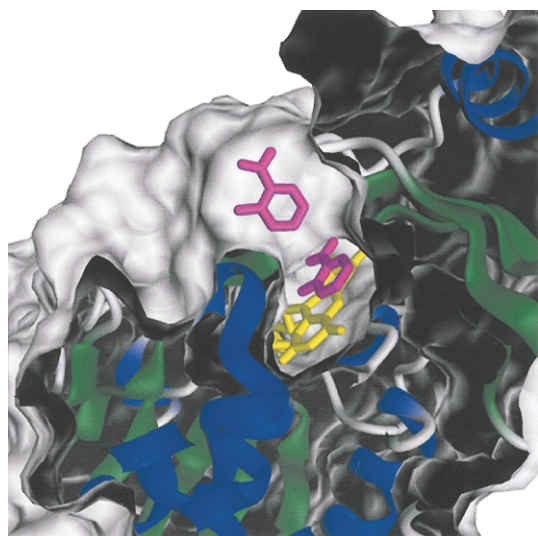
Figure 6. Molecular surface representation of the DAAO–anthranilate complex showing a magnified view of the funnel leading to the active site. The protein main-chain is shown as a coloured ribbon according to the domain colouring shown in Figure 1. The anthranilate and FAD molecules are depicted in magenta and yellow, respectively. One anthranilate molecule is bound into the active site in close contact with the flavin, whereas the plane of the second is parallel with that of the aromatic side-chain of Tyr238 (see also Figures 4(b) and 5). The surface map was produced with the program DINO†.

controlled by the orientation of the phenolic ring of Tyr238 (see above), and also provides a surface suitable to interact with non-polar and aromatic compounds (and substrates).

Discussion

On the basis of the data presented here, we propose that yeast DAAO dimerizes in a head to tail mode (see Figure 1 and compare with Figure 3) involving parts of loop 302–322 (βF5–βF6). This would be in line with results from limited proteolysis carried out with RgDAAO,[24,34] which show that disruption of this loop abolishes the capacity to dimerize. The peptide bonds at Thr306 and Arg318 (Figure 1) of the mentioned loop are susceptible to trypsin, chymotrypsin and thermolysin proteolysis[24,34] leading in all cases to active, monomeric holoenzyme containing two polypeptides of ~34 kDa (Met1–Arg305 or Met1–Leu312) and of ~5 kDa (Ala319–Ala362).[24,34] This mode of dimerization yields a quasi-spherical particle and, due to the large contact area, should result in a stable dimeric protein. This is different from the head to head mode proposed for mammalian DAAO,[10] where the interaction is much weaker, and activity depends upon the aggregation state of the protein in solution.[9]

Flavoenzymes are often equipped with flexible elements, which have a role in controlling the accessibility of the active site.[35] In pkDAAO a loop, formed by residues 216–228, acts as a lid, which swings between an "open" and "closed" conformation to allow access/release of substrate/product.[32] This conformational change is comparatively slow and controls the overall rate of turnover of the mammalian enzyme, where product release is rate-limiting.[8] In yeast DAAO a corresponding loop that could exert the same function is not present; however, Tyr238 in a rudimentary fashion, appears to play a comparable role. The side-chain of this amino acid is assumed to take the open conformation in uncomplexed enzyme, and this might initiate an interaction with substrate, leading it into the bottom of the active site (Figure 6). Then, concomitantly with a conformational change positioning it further inside the active site, it contributes to the fixation of the substrate –COO⁻ in a position suitable for catalysis (see the different conformations of Tyr238 in Figure 4(a) and (b)). This is in agreement with the results obtained with RgDAAO Tyr238Phe and Tyr238Ser mutants, indicating that the main function of this group is in substrate/product exchange instead of in binding (the K_m value for the D-amino acid, as well the K_d value for ligand binding, are only slightly altered by the substitutions) (L.P., unpublished results).

A salient feature of the active site pocket is the presence of a wide cavity where the side-chain of the substrate can be accommodated (Figures 4 and 6). This provides a rationale for the preference of RgDAAO for D-amino acid residues carrying an aromatic and/or hydrophobic side-chain, compared to polar ones,[4,9] and for its capacity to accommodate large residues, as in the case of cephalosporins.[6] It also explains the reluctance of RgDAAO to act on amino acid residues carrying a polar and, in particular, a charged side-chain. The use of a single side-chain to control the accessibility of the active site has been observed also in UDP-*N*-acetylenolpyruvoyl-glucosamine reductase.[36] In analogy to LAAO, where three anthranilate molecules are present in each protomer inside the channel leading to the active site,[17] the position of the two anthranilate molecules found in RgDAAO is taken to reflect the trajectory of the substrate from the surface to the locus of the catalytic event (Figures 4 and 6). The one anthranilate in contact with the flavin occupies the position assumed by normal D-amino acid substrates. The second one is in contact with Tyr238, and its amino group is positioned directly above the tyrosine ring. It is tempting to hypothesize that D-amino acid residues entering the active site behave similarly: their cationic ammonium group would undergo a cation–π-interaction[37] and this could contribute substantially to the binding energy. Upon moving to the second binding site at the bottom of the active centre, depending on the pH the ammonium group would deprotonate[12] in order to undergo

catalysis. Such a π-interaction might be absent or reduced in the product, since the imino/immonium group readily hydrolyses (see equation (3)). After catalysis, and if imino acid hydrolysis occurs prior to dissociation, the product cannot be retained by π-interaction and would thus freely diffuse away. If this hypothesis holds, the "second" substrate site at the entrance of the cavity would act like a valve. The observed rotation of the Tyr238 side-chain would simply be effected by an induced fit mechanism, which optimally positions substrate and tyrosine ring with respect to each other.

An interesting feature of DAAOs and of flavoprotein oxidases in general is their ability to stabilize a negative charge on the flavin where it is localized mainly in the pyrimidine ring. This is the case, e.g. upon reduction (see equation (1)), with semiquinones,[29] with modified flavins,[28] and also in the case of sulphite binding.[9,27] This stabilization translates into an increase in redox potential, a feature of most flavoprotein oxidases.[38] With flavocytochrome b_2 and related enzymes that dehydrogenate α-OH acids, a lysine ε-NH_3^+ located near the flavin N(1) brings about this stabilization.[39] In pkDAAO an α-helix dipole has been proposed to be involved in this stabilization.[10] With RgDAAO, however, no arrangement of (partial) positive charges that could have a similar role is evident from the 3D structure. This thus raises the question about the mechanism of stabilization in RgDAAO: two cases can be differentiated. In the first, substrate dehydrogenation (equation (1)) contains the equilibrium of the two Michaelis complexes at the levels of oxidized and reduced enzyme as depicted in equation (4):

$$\{DAAO \sim FAD_{ox} \sim R-CH(-NH_2)-COO^-\}$$

$$\Leftrightarrow \{DAAO \sim FAD_{red}H^-$$

$$\sim R-C(=NH_2^+)-COO^-\} \qquad (4)$$
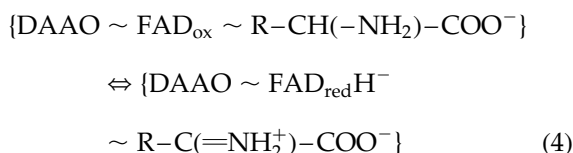
(Note that a H^+ from the α-amino group is released prior/concomitantly with the dehydrogenation, i.e. the "NH_2 form" of bound amino acid is the one that reacts efficiently.[12])

In equation (4) the stabilization of negatively charged, reduced flavin is by the positively charged α-imino (α=NH_2^+) product.[12] The latter is positioned above the flavin pyrimidine ring and in an ideal position to stabilize its negative charge.[12] The second case occurs when the positive charge associated with the ligand is absent: to account for stabilization we proposed that Arg285 plays a dual role.[14] In the presence of a ligand having a carboxylic group it serves in its binding. In its absence, the guanidinium side-chain of Arg285 rotates around the $C^ε$ bond to come in close proximity (∼3 Å) to the flavin pyrimidine ring and above its plane, where it can exert a neutralizing function. Modelling studies show that with pkDAAO the equivalent Arg283 can do the same

(not shown). We would thus infer that also with pkDAAO the stabilization of negatively charged flavin species results primarily from the interaction with this Arg, whereby the invoked helix dipole[10] can play an ancillary role.

Comparison of the structures of DAAO and LAAO[17] demonstrates that the groups involved in binding of the substrate αCOO^- and αNH_2 groups (interactions (a) and (b), see Results) form a mirror plane intersecting the axis formed by the substrate αC−H function and the flavin N(5) position. The discrimination by DAAO and LAAOs towards D and L-enantiomers can thus be rationalized in terms of a classical three-point attachment model (interactions (a), (b) and (c), above). This also would be equivalent to the four-location model recently discussed by Koshland:[40] the fourth site being a direction, i.e. the orientation of the αC−H orbital with respect to flavin N(5) HOMO orbital. In LAAO and pkDAAO, the ligand amino group interacts with the carbonyl oxygen atom of a conserved glycine (Gly464 and Gly313, respectively), which is located at the same position as Ser335 in RgDAAO. Recently, the hydroxyl group of Ser335 has been proposed to play a role in transfer of a H^+ to bulk solvent,[16] a function possibly carried out by His223 in LAAO.[17] A further intriguing difference between DAAO and LAAO is the presence in the latter of a water molecule (W605) H-bonded to the flavin N(5) and to the side-chain of Lys326.[17] It has been suggested that Lys326 is involved in hydrolysis of the imino product by Trp605. Clearly such a mechanism would not appear to be viable in RgDAAO, due to the absence of analogous groups.

Some interesting similarities exist also with D-amino acid aminotransferase (D-AAT), a bacterial enzyme capable of transaminating D-amino acid residues and important for synthesis of D-glutamate and D-alanine, which are components of the bacterial cell wall. Also in this enzyme an extended loop (Gly94−Pro109) is important for the monomer−monomer contact (and provides residues to the cofactor-binding region and active site).[41] Both DAAO and D-AAT recognize D-amino acid residues as substrates and possess a "carboxylate trap" (Arg285 in RgDAAO and Arg98 in D-AAT) and a "side-chain pocket" that discriminates substrate species. This cavity forms a pocket in which the side-chain of the substrate can be trapped and provides a surface for interaction with the side-chain.

In conclusion, comparison of the 3D structures of yeast and mammalian DAAO suggests that evolutive pressure has led to two enzymes that share the same chemical process, but use different kinetic mechanisms for catalysis. In the case of RgDAAO, and as a consequence of catabolic requirements, optimal catalytic efficiency has evolved leading to the (chemical) step of hydride transfer being rate-limiting. With mammalian DAAO we assume that the necessity to regulate activity has caused product release to be limiting. This diversity is

Table 2. Data collection and refinement

A. Diffraction data

Redox state of flavin	Oxidized
Resolution (Å)	100–1.9 (2.0–1.9)
Cell axes (Å)	$a = b = 120.8; c = 136.8$
Observed reflections	193, 503
Unique reflections	75,551
Completeness (%)	99.0 (99.8)
R_{mgr-F}[51]	13.8 (28.7)
I/σ	5.3 (1.9)

B. Refinement

R-factor/R-free (%)	20.5/24.8
No. of protein atoms	2799
Solvent molecules with full occupancy	254
Solvent molecules with half occupancy	118
Substrates, ligands, and cofactor	2 anthranilates, FAD
Model r.m.s. deviations from ideality[a]	
Bond lengths (Å)	0.018
Bond angles (°)	3.21

Parentheses denote the highest shell.
[a] Calculations performed with SHELXPRO.[44]

implemented by the use of different types of "lids" that cover the active site and are involved in uptake and release of ligand.

Materials and Methods

Preparation of the protein and crystallization

Wild-type RgDAAO was expressed and purified in *Escherichia coli* using the pT7-DAAO expression system in BL21(DE3)pLysS *E. coli* cells. The purified DAAO is stable in the 0.1–10 mg/ml protein concentration range and has spectral and kinetic properties identical with those of native enzyme.[19] The purified protein was concentrated up to 10 mg/ml and equilibrated in 20 mM Hepes buffer at pH 7.5 by gel-permeation chromatography on a Sephadex G-25 (PD10) column. The dynamic light-scattering analysis was performed with model DynaPro 801 (Protein Solutions, Ltd). The recombinant form of RgDAAO was crystallized by vapour diffusion method at 20 °C, as reported.[12] The crystals obtained by this method were found to contain L-lactate in variable amounts. The source of this ligand was found to be a lactate contamination (≈ 0.4 g/kg) of commercial PEG1000 (FLUKA). The RgDAAO–anthranilate complex was obtained by soaking the crystals in the pure cryo-protection solution containing 30 mM of the ligand. Binding was followed by observation of the crystal colour changes from yellow to reddish, this being complete within one minute.

Solution of the RgDAAO crystal structure

The anthranilate dataset was collected under cryogenic conditions. Prior to flash freezing, the crystals were transferred into the cryo-protectant solution, consistent with the reservoir solution and 20% (v/v) glycerol. Data collection was on a rotating anode source (Schneider, Offenburg, Germany) using the MAR345 image plate system. Space group determination and data reduction was carried out in XDS.[42] The refined model omitting L-lactate was the starting point for solving the structure of RgDAAO in anthranilate complex. The refinement employed a torsion angle dynamics[43] at a starting temperature of 5000 K. Refinement was continued with SHELXL.[44] The restraints were set in accordance with the resolution of the data and continuous control of the stereochemical quality of the structures was done with PROCHECK.[45] For details of data collection statistics and refinement see Table 2. Structure plots were produced with the programs MOLSCRIPT[46] and Raster3D.[47]

Comparison of GR family members

A superposition calculation was performed for each member of the GR_2 family using the program Superimpose[48] and parameters describing the superposition were extracted with lsqman[49] from the best topological superposition.

Accession numbers

The coordinates and structure factors are deposited in the RCSB Protein Data Bank under accession code 1c0i.

References

1. Krebs, H. A. (1935). Metabolism of amino-acids. III. Deamination of amino-acids. *Biochem. J.* **29**, 1620–1644.
2. La Rue, T. A. & Spencer, J. F. T. (1967). The utilization of D-amino acids by yeasts. *Can. J. Microbiol.* **13**, 777–788.
3. Pilone, M. S., Verga, R., Fretta, A. & Hanozet, G. M. (1989). Induction of D-amino acid oxidase by D-alanine in *Rhodotorula gracilis* grown in defined medium. *J. Gen. Microbiol.* **135**, 593–600.
4. Pilone, M. S. (2000). D-Amino acid oxidase: new findings. *Cell. Mol. Life Sci.* **57**, 1732–1747.
5. Schell, M. J., Molliver, M. E. & Snyder, S. H. (1995). D-Serine, an endogenous synaptic modulator: localization to astrocytes and glutamate-stimulated release. *Neurobiology*, **92**, 3948–3952.
6. Pilone, M. S. & Pollegioni, L. (2002). D-Amino acid oxidase as an industrial biocatalyst. *Biocatal. Biotransf.* **20**, 145–159.
7. Pollegioni, L., Langkau, B., Tischer, W., Ghisla, S. & Pilone, M. S. (1993). Kinetic mechanism of D-amino acid oxidase from *Rhodotorula gracilis* and *Trigonopsis variabilis*. *J. Biol. Chem.* **268**, 13850–13857.
8. Porter, D. J. T., Voet, J. G. & Bright, H. J. (1977). Mechanistic features of the D-amino acid oxidase reaction studied by double stopped flow spectrophotometry. *J. Biol. Chem.* **252**, 4464–4473.

9. Curti, B., Ronchi, S. & Pilone Simonetta, M. (1992). D- and L-amino acid oxidases. In *Chemistry and Biochemistry of Flavoenzymes* (Müller, F., ed.), vol. 3, pp. 69–94, CRC Press, Boca Raton.

10. Mattevi, A., Vanoni, M. A., Todone, F., Rizzi, M., Teplyakov, A., Coda, A. *et al.* (1996). Crystal structure of D-amino acid oxidase: a case of active site mirror-image convergent evolution with flavocytochrome b_2. *Proc. Natl Acad. Sci. USA*, **93**, 7496–7501.

11. Mizutani, H., Miyahara, I., Hirotsu, K., Nishina, Y., Shiga, K., Setoyama, C. & Miura, R. (1996). Three-dimensional structure of porcine kidney D-amino acid oxidase at 3.0 Å resolution. *J. Biochem. (Tokyo)*, **120**, 14–17.

12. Umhau, S., Pollegioni, L., Molla, G., Diederichs, K., Welte, W., Pilone, M. S. & Ghisla, S. (2000). The X-ray structure of D-amino acid oxidase at very high resolution identifies the chemical mechanism of flavin-dependent substrate dehydrogenation. *Proc. Natl Acad. Sci. USA*, **97**, 12463–12468.

13. Harris, C. M., Molla, G., Pilone, M. S. & Pollegioni, L. (1999). Studies on the reaction mechanism of *Rhodotorula gracilis* D-amino acid oxidase: role of the highly conserved Tyr223 on substrate binding and catalysis. *J. Biol. Chem.* **274**, 36235–36240.

14. Molla, G., Porrini, D., Job, V., Motteran, L., Vegezzi, C., Campaner, S. *et al.* (2000). Role of arginine 285 in the active site of *Rhodotorula gracilis* D-amino acid oxidase. *J. Biol. Chem.* **275**, 24715–24721.

15. Pollegioni, L., Blodig, W. & Ghisla, S. (1997). On the mechanism of D-amino acid oxidase. Structure/linear free energy correlations and deuterium kinetic isotope effects using substituted phenylglycines. *J. Biol. Chem.* **272**, 4924–4934.

16. Harris, C. M., Ghisla, S. & Pollegioni, L. (2001). pH and kinetic effects in D-amino acid oxidase catalysis. Evidence for a concerted mechanism in substrate dehydrogenation *via* hydride transfer. *Eur. J. Biochem.* **268**, 1–18.

17. Pawelek, P. D., Cheah, J., Coulombe, R., Macheroux, P., Ghisla, S. & Vrielink, A. (2000). The structure of L-amino acid oxidase reveals the substrate trajectory into an enantiomerically conserved active site. *EMBO J.* **19**, 4204–4215.

18. Miura, R., Setoyama, C., Nishina, Y., Shiga, K., Mizutani, H., Miyahara, I. & Hirotsu, K. (1997). Structural and mechanistic studies on D-amino acid oxidase–substrate complex: implications of the crystal structure of enzyme–substrate analog complex. *J. Biochem. (Tokyo)*, **122**, 825–829.

19. Molla, G., Vegezzi, C., Pilone, M. S. & Pollegioni, L. (1998). Overexpression in *Escherichia coli* of a recombinant chimeric *Rhodotorula gracilis* D-amino acid oxidase. *Prot. Express. Purif.* **14**, 289–294.

20. Faotto, L., Pollegioni, L., Ceciliani, F., Ronchi, S. & Pilone, M. S. (1995). The primary structure of D-amino acid oxidase from *Rhodotorula gracilis*. *Biotechnol. Letters*, **17**, 193–198.

21. Macheroux, P., Seth, O., Bollschweiler, C., Schwarz, M., Kurfürst, M., Au, L. C. & Ghisla, S. (2001). L-amino-acid oxidase from the Malayan pit viper *Calloselasma rhodostoma*. Comparative sequence analysis and characterization of active and inactive forms of the enzyme. *Eur. J. Biochem.* **268**, 1679–1686.

22. Rossmann, M. G., Moras, D. & Olsen, K. W. (1974). Chemical and biological evolution of nucleotide-binding proteins. *Nature*, **250**, 194–199.

23. Dyn, O. & Eisenberg, D. (2001). Sequence-structure analysis of FAD-containing proteins. *Protein Sci.* **10**, 1712–1728.

24. Campaner, S., Pollegioni, L., Ross, B. & Pilone, M. S. (1998). Limited proteolysis and site-directed mutagenesis revealed the origin of microheterogeneity of *Rhodotorula gracilis* D-amino acid oxidase. *Biochem. J.* **330**, 615–621.

25. Wierenga, R. K., Drenth, J. & Schulz, G. E. (1983). Comparison of the three-dimensional protein and nucleotide structure of the FAD-binding domain of *p*-hydroxybenzoate hydroxylase with the FAD- as well as NADPH-binding domains of glutathione reductase. *J. Mol. Biol.* **167**, 725–739.

26. Schulz, G. E. (1992). Binding of nucleotides by proteins. *Curr. Opin. Struct. Biol.* **2**, 61–67.

27. Fraaije, M. W. & Mattevi, A. (2000). Flavoenzymes: diverse catalysts with recurrent features. *Trends Biochem. Sci.* **25**, 126–132.

28. Pollegioni, L., Ghisla, S. & Pilone, M. S. (1992). Studies on the active center of *Rhodotorula gracilis* D-amino acid oxidase and comparison with pig kidney enzyme. *Biochem. J.* **286**, 389–394.

29. Pilone, M. S., Pollegioni, L., Casalin, P., Curti, B. & Ronchi, S. (1989). Properties of D-amino-acid oxidase from *Rhodotorula gracilis*. *Eur. J. Biochem.* **180**, 199–204.

30. Casalin, P., Pollegioni, L., Curti, B. & Pilone, M. S. (1991). A study on apoenzyme from *Rhodotorula gracilis* D-amino acid oxidase. *Eur. J. Biochem.* **197**, 513–517.

31. Brünger, A. T., Adams, P. D., Clore, G. M., DeLano, W. L., Gros, P., Grosse-Kunstleve, R. W. *et al.* (1998). Crystallographic and NMR system: a new software suite for macromolecular structure determination. *Acta Crystallog. sect. D*, **54**, 905–921.

32. Todone, F., Vanoni, M. A., Mozzarelli, A., Bolognesi, M., Coda, A., Curti, B. & Mattevi, A. (1997). Active site plasticity in D-amino acid oxidase: a crystallographic analysis. *Biochemistry*, **36**, 5853–5860.

33. Pollegioni, L., Fukui, K. & Massey, V. (1994). Studies on the kinetic mechanism of pig kidney D-amino acid oxidase by site-directed mutagenesis of tyrosine 224 and tyrosine 228. *J. Biol. Chem.* **269**, 31666–31673.

34. Pollegioni, L., Ceciliani, F., Curti, B., Ronchi, S. & Pilone, M. S. (1995). Studies on the structural and functional aspects of *Rhodotorula gracilis* D-amino acid oxidase by limited proteolysis. *Biochem. J.* **310**, 577–583.

35. Mattevi, A., Vanoni, M. A. & Curti, B. (1997). Structure of D-amino acid oxidase: new insights from an old enzyme. *Curr. Opin. Struct. Biol.* **7**, 804–810.

36. Benson, T. E., Filman, D. J., Walsh, C. T. & Hogle, J. M. (1995). An enzyme–substrate complex involved in bacterial cell wall biosynthesis. *Nature Struct. Biol.* **2**, 644–653.

37. Mecozzi, S., West, A. P., West, L. & Dougherty, D. A. (1996). Cation–pi interactions in aromatics of biological and medicinal interest: electrostatic potential surfaces as a useful qualitative guide. *Proc. Natl Acad. Sci. USA*, **93**, 10566–10571.

38. Edmondson, D. & Ghisla, S. (1999). Flavoenzyme structure and function. Approaches using flavin analogues. *Methods Mol. Biol.* **131**, 157–179.

39. Xia, Z.-X., Shamala, N., Bethge, P. H., Lim, L. W., Bellamy, H. D., Xuong, N. H. *et al.* (1987). Three-dimensional structure of flavocytochrome b_2 from baker's yeast at 3.0 Å resolution. *Proc. Natl Acad. Sci. USA*, **84**, 2629–2633.

40. Mesecar, A. D. & Koshland, D. E., Jr (2000). A new model for protein stereospecificity. *Nature*, **403**, 614–615.

41. Sugio, S., Petsko, G. A., Manning, J. M., Soda, T. & Ringe, D. (1995). Crystal structure of a D-amino acid aminotransferase: how the protein controls stereo-selectivity. *Biochemistry*, **34**, 9661–9669.

42. Kabsch, W. J. (1988). Evaluation of single crystal X-ray diffraction from a position-sensitive detector. *J. Appl. Crystallog. sect. A*, **50**, 157–163.

43. Brünger, A. T., Adams, P. D. & Rice, L. M. (1997). New applications of simulated annealing in X-ray crystallography and solution NMR. *Structure*, **15**, 325–336.

44. Sheldrick, G. M. & Schneider, T. R. (1997). SHELXL: high-resolution refinement. *Methods Enzymol.* **277**, 319–343.

45. Laskowski, R. A., MacArthur, M. W., Moss, D. S. & Thornton, J. M. (1993). PROCHECK: a program to check the stereochemical quality of protein structures. *J. Appl. Crystallog.* **26**, 283–291.

46. Kraulis, P. J. (1991). MOLSCRIPT: a program to produce both detailed and schematic plots of protein structures. *J. Appl. Crystallog.* **24**, 946–950.

47. Merrit, E. A. & Murphy, M. E. P. (1994). Raster3D version 2.0. A program for photorealistic molecular graphics. *Acta Crystallog. sect. D*, **50**, 869–873.

48. Diederichs, K. (1995). Structural superposition of proteins with unknown alignment and detection of topological similarity using a six-dimensional search algorithm. *Proteins: Struct. Funct. Genet.* **23**, 187–195.

49. Kleywegt, G. J. (1999). Experimental assessment of differences between related protein crystal structures. *Acta Crystallog. sect. D*, **55**, 1857–1884.

50. Diederichs, K. (2000). Computing in macromolecular crystallography using a parallel architecture. *J. Appl. Crystallog.* **33**, 1154–1161.

51. Diederichs, K. & Karplus, P. A. (1997). Improved *R*-factors for diffraction data analysis in macro-molecular crystallography. *Nature Struct. Biol.* **4**, 269–275.